Research Square

Preprints are preliminary reports that have not undergone peer review.
They should not be considered conclusive, used to inform clinical practice,
or referenced by the media as validated information.

Statistical Shape Model–based Refinement of Dental Surface Geometries for Digital Manufacturing Workflows

Giuliana Baiamonte

giuliana.baiamonte@unict.it

University of Catania: Universita degli Studi di Catania

Michele Calì
Luca Di Angelo
Fulvia Concetta Rita Monaco
Antonio Marzola

Research Article

Keywords: 3D Medical Image Analysis, Surface Reconstruction, Enhanced Statistical Shape Model, Dental Surface Reconstruction, Automated Geometric Modelling

Posted Date: July 2nd, 2026

DOI: https://doi.org/10.21203/rs.3.rs-9556642/v1

License: This work is licensed under a Creative Commons Attribution 4.0 International License.
Read Full License

Statistical Shape Model–based Refinement of Dental Surface Geometries for Digital Manufacturing Workflows

Giuliana Baiamonte[1*], Michele Calì[1], Luca Di Angelo[2], Fulvia Concetta Rita Monaco[1], Antonio Marzola[2]

Abstract

Digital manufacturing workflows in dentistry require accurate and anatomically consistent tooth models derived from heterogeneous acquisition modalities. However, preliminary tooth segmentations obtained from CBCT or intraoral scanning often exhibit incomplete or ambiguous regions, particularly at interdental contacts, which can compromise downstream design and manufacturing processes. This work presents a fully automated, anatomy-aware refinement pipeline based on an enhanced Statistical Shape Model, designed as a post-processing stage for preliminary tooth reconstructions. The method integrates target geometries with population-based anatomical priors, explicitly preserving reliable surface regions while reconstructing uncertain or missing areas through a globally constrained statistical deformation. Semantic anatomical information embedded in the eSSM enables contact-aware refinement relevant to design-oriented applications. The pipeline was evaluated on adult maxillary first molars using target models derived from both CBCT-based segmentations and intraoral scans. The results demonstrate that the proposed approach produces complete, smooth, and anatomically plausible tooth models while maintaining fidelity to the observed geometry. The refined reconstructions are directly suitable for downstream manufacturing-related applications, reducing manual intervention and improving robustness within digital dental workflows.

Keywords 3D Medical Image Analysis, Surface Reconstruction, Enhanced Statistical Shape Model, Dental Surface Reconstruction, Automated Geometric Modelling.

✉ Giuliana Baiamonte
giuliana.baiamonte@unict.it

Michele Calì
michele.cali@unict.it

Luca Di Angelo
luca.diangelo@univaq.it

Fulvia Concetta Rita Monaco
fulvia.monaco@unict.it

Antonio Marzola
antonio.marzola@univaq.it

[1] Electric, Electronics and Computer Engineering Department, University of Catania, Catania, Italy

[2] Department of Industrial and Information Engineering and Economics, University of L'Aquila, L'Aquila, Italy

1 Introduction

The progressive adoption of fully digital workflows in contemporary dentistry has profoundly transformed planning, design, and manufacturing stages, increasing the demand for accurate and reliable three-dimensional models of individual teeth [1, 2]. In digital manufacturing pipelines, the digital tooth model serves as a geometric reference for a broad range of downstream operations, from treatment planning to the design and fabrication of patient-specific devices such as surgical guides [3].

Consequently, the geometric quality and anatomical plausibility of this model directly affect design robustness, manufacturing tolerances, and the reliability of the final clinical outcome [4, 5]. Current acquisition technologies enable the digitization of dental anatomy either as volumetric data or surface representations, depending on clinical and manufacturing requirements [6, 7]. Cone-beam computed tomography (CBCT) is widely used to capture the complete tooth anatomy, providing high-resolution volumetric datasets at relatively low radiation doses [8, 9]. In contrast, intraoral scanners provide a reliable tool for digitizing external morphology, enabling fast, non-invasive surface acquisition [10, 11]. Regardless of the modality, the acquired data are ultimately converted into digital geometric models, typically surface meshes in STL format, which constitute the starting point for subsequent planning, design, and manufacturing processes [12]. Despite continuous technological advances, generating accurate and complete digital tooth models remains challenging, particularly for posterior teeth such as molars [13]. Complex crown morphology, tight interproximal contacts, occlusal superposition, and proximity to adjacent teeth often limit the quality of both acquisition and segmentation processes [14].

These issues are exacerbated by other critical aspects related to the acquisition technology, such as imaging artefacts, partial-volume effects, beam hardening in CBCT, occlusions, and stitching errors in surface scanning. As a result, preliminary digital models often contain incomplete, ambiguous, or geometrically inconsistent regions, especially in critical areas affecting functional and manufacturing accuracy. When such defects are propagated through digital workflows, they can

compromise the geometric accuracy of surgical devices (especially surgical guides that rely directly on existing teeth for positioning), affect occlusal relationships, and ultimately reduce the reliability and reproducibility of manufacturing outcomes. In this context, refining digital tooth geometries is a critical step not only for anatomical reconstruction but also for ensuring geometric consistency and manufacturability in downstream CAD/CAM workflows. In recent years, automatic tooth segmentation has increasingly relied on data-driven approaches, especially deep learning (DL)–based methods [15].

Convolutional neural networks, and U-Net–derived architectures in particular, have demonstrated high accuracy and computational efficiency in dental structure labeling and segmentation, often outperforming classical image-processing techniques such as thresholding, region growing, deformable models, and morphological operations [16, 17]. Reported Dice similarity coefficients approaching 0.93 confirm the effectiveness of these approaches under favorable imaging conditions [18, 19]. However, DL-based methods implicitly encode anatomical plausibility through the training data, making their performance highly dependent on the availability of large datasets of complete, anatomically correct teeth [20]. Such datasets remain limited, especially for posterior regions affected by interproximal contacts [21]. Consequently, even advanced segmentation strategies often yield preliminary models that are unsuitable as reliable geometric references for manufacturing-oriented workflows. From an advanced manufacturing perspective, this limitation highlights the need for a dedicated refinement step able to transform a coarse or imperfect digital tooth model into a geometrically consistent and anatomically plausible representation. Such a refinement must be capable of mitigating the effects of acquisition artefacts, segmentation inaccuracies, and missing or ambiguous surface information, without compromising the geometric fidelity of the portions that are reliably captured by the imaging or scanning process.

This objective cannot be achieved by enforcing point-These wise corrections or purely local adjustments, as these approaches tend to propagate noise and inconsistencies present in the input data. Instead, the reconstruction must be formulated as a global shape estimation problem, in which the final
geometry is inferred as a coherent deformation of a complete anatomical template. Within this framework, the available geometric information helps constrain the solution, while the overall shape evolution is governed by anatomical consistency across the entire tooth.

Existing tooth reconstruction and shape completion methods can be broadly classified into three main categories: computer-aided design (CAD)–based reconstruction approaches relying on local geometric interpolation, multimodal fusion strategies that combine volumetric imaging with high-resolution surface acquisitions to reconstruct complete tooth models, and population-based techniques that leverage statistical anatomical priors to infer globally consistent shapes from incomplete observations [22].

CAD-based methods typically rely on local geometric continuity, curvature constraints, or manually defined control points to interpolate missing regions. While parametric representations such as B-splines and Non-Uniform Rational B-Splines (NURBS) are mathematically robust and compatible with industrial design environments [23-26], they often struggle to reproduce fine anatomical details such as cusps, fissures, and ridges without extensive manual intervention. This frequently leads to over-smoothing, unstable fittings, or operator-dependent results that are incompatible with automated manufacturing pipelines [27, 16].

Multimodal fusion strategies attempt to overcome the limitations of single-modality reconstructions by combining complementary information from volumetric imaging and high-resolution surface acquisitions. Typically, CBCT data provide complete tooth–bone structures, including roots, while intraoral or laser scans offer highly accurate crown morphology and occlusal information. The fusion process generally involves segmentation of CBCT volumes, registration between modalities, and replacement of the crown region reconstructed from CBCT with the high-resolution surface mesh, followed by stitching and smoothing to obtain a complete tooth model [28, 29]. These approaches aim to mitigate well-known CBCT limitations, such as low resolution, tooth crowding, and occlusal contact artefacts, which often lead to inaccurate crown reconstruction. By integrating intraoral scans, multimodal pipelines improve crown accuracy while preserving root information derived from CBCT data [28, 29]. However, multimodal fusion methods typically rely on accurate segmentation and registration between modalities, which remain challenging due to differences in bite position, connected boundaries between adjacent teeth, and discrepancies in shape between CBCT reconstructions and intraoral meshes. Moreover, several approaches rely on fiducial-based or surface-based alignment procedures and may still require manual interaction or heuristic stitching steps, limiting full automation and anatomical consistency [29, 30].

Population-based approaches address these limitations by explicitly leveraging prior anatomical knowledge learned from a cohort of shapes. Within this category, both artificial intelligence (AI)–based generative models and Statistical Shape Models (SSMs) have been proposed. While generative AI approaches typically require large training datasets, SSMs offer a compact, interpretable, and mathematically grounded representation of anatomical

variability, enabling robust inference even with limited training data [31]. SSMs have been successfully applied to anatomical modelling tasks such as segmentation, reconstruction, and morphometric analysis, including several applications in dental modelling under incomplete or occluded data conditions [32-38]. Enhanced Statistical Shape Models (eSSMs) further extend the SSM framework by incorporating additional information beyond pure geometry while maintaining robustness and generalisation [39].

Building on these considerations, the present work proposes an enhanced Statistical Shape Model (eSSM)–based framework for refining and completing single-tooth digital models, specifically targeting the generation of anatomically coherent geometries suitable for downstream CAD/CAM and advanced manufacturing workflows. The proposed eSSM is trained on complete segmentations of a specific tooth class and encodes anatomically plausible shape variability as an explicit morphological prior. Rather than acting as a standalone segmentation method, the proposed framework is designed as a population-based refinement strategy that complements existing acquisition and segmentation pipelines. Specifically, it addresses the limitations of CAD-based interpolation and purely data-driven approaches in handling incomplete or anatomically ambiguous regions by operating on a preliminary digital model represented as either a surface mesh or a point cloud, independently of its origin. The framework distinguishes between morphologically reliable and ambiguous regions within the initial model by evaluating geometric consistency with the statistical prior, including surface orientation and local shape coherence. Reliable regions are preserved to maintain fidelity to the acquired data, while ambiguous areas are refined through a global, statistically guided estimation that enforces anatomical consistency. In addition, the eSSM is constructed tooth-class-specifically and embeds semantic anatomical information at the vertex level, enabling automatic partitioning of the reconstructed model into meaningful anatomical regions relevant for downstream design and manufacturing tasks. The feasibility of the proposed approach is demonstrated on a test set comprising both CBCT- and intraoral-scan–derived molars. This choice represents a challenging, clinically relevant scenario. It does not limit the applicability of the framework to other tooth types or, more generally, to digital reconstruction problems in advanced manufacturing workflows that require anatomically coherent geometric models.

2 Methods

2.1 Overview of the complete pipeline

In this work, the reconstruction of individual teeth is performed through an anatomy-aware refinement pipeline based on an eSSM, which integrates preliminary segmentation data with population-based anatomical priors. An overview of the workflow is reported in Figure 1. The pipeline takes as input a preliminary reconstruction of the target tooth, represented as either a point cloud or a triangulated surface mesh. This initial geometry may come from various acquisition methods and segmentation strategies and is not limited by the specific techniques used in the earlier stages. A key aspect of the proposed framework is the identification of surface regions that are weakly constrained by the acquired data and therefore prone to geometric ambiguity. Such regions typically arise in areas affected by partial-volume effects, beam-hardening artefacts, limited image contrast, scanning occlusions, or at interdental contact areas, where the superposition of adjacent teeth prevents a reliable delineation of anatomical boundaries [40]. Inaccurate reconstruction of these regions may propagate through downstream workflows, leading to clinically and manufacturing-relevant issues, such as improper fit of tooth-supported devices. To account for these limitations, each surface point of the preliminary reconstruction is associated with a binary confidence indicator reflecting the degree of reliability of the underlying geometric information; this classification is derived from (i) the spatial relationship with neighboring teeth, identifying regions likely affected by contact ambiguity, and (ii) local geometric consistency with the anatomical variability encoded by the eSSM. Points exhibiting ambiguous boundary information or implausible surface orientation are treated as weakly constrained, while well-defined regions are preserved. Shape completion is then achieved by fitting the eSSM to the subset of points associated with reliable geometric information. The fitting is formulated as an iterative Maximum A Posteriori (MAP) estimation problem, which enforces consistency with the observed data while regularizing the solution through a global anatomical prior. At each iteration, a complete tooth geometry is inferred, including regions not directly supported by the data, enabling progressive refinement of the reconstruction until convergence. The resulting model preserves the fidelity of well-segmented areas while completing ambiguous regions in a smooth, anatomically plausible, and statistically consistent manner. In addition to geometric information, the eSSM encodes semantic anatomical labels at the vertex level, allowing the automatic partitioning of the reconstructed tooth into meaningful regions for quantitative analysis, simulation, and design-oriented applications. The individual components of the proposed pipeline are described in detail in the following sections.

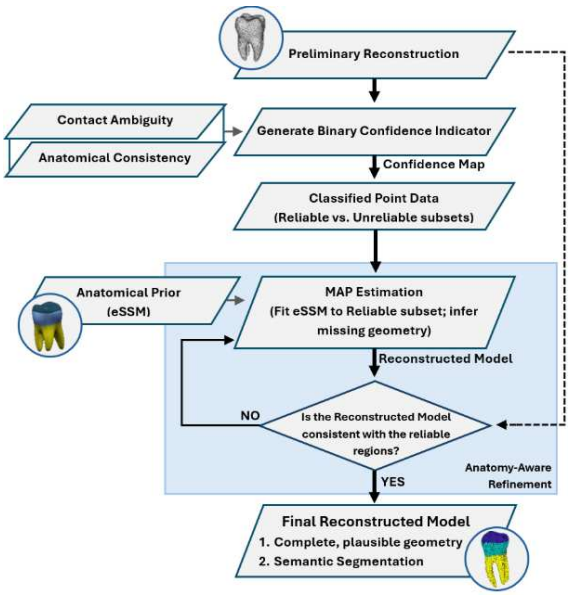


Fig. 1 The proposed pipeline

2.2 The enhanced Statistical Shape Model

The proposed eSSM builds upon the classical SSM, a well-established framework that models anatomical variability by representing each shape as a deformation of a mean shape along principal modes learned from a training population. In this study, the eSSM is trained on an anatomically consistent dataset consisting of complete tooth segmentations derived from CBCT volumes, restricted to a specific tooth class. CBCT data were selected because they provide volumetric information of the entire tooth anatomy with sufficient spatial resolution, including regions that are typically inaccessible to surface-based acquisition techniques. Following a standard PCA-based formulation, all M training samples are first brought into dense point-wise correspondence, such that each shape is represented by the same number of vertices and homologous anatomical locations are consistently aligned across the population [41]. The resulting statistical model captures population-level variability of tooth morphology while preserving anatomical plausibility across the full three-dimensional structure. Each shape is stored as an $N \times 3$ matrix of Cartesian coordinates $\mathbf{x} = (x, y, z)$ and vectorized by stacking the coordinate components into a single shape vector:

$$\mathbf{s}_k = [x_1, \dots, x_N, y_1, \dots, y_N, z_1, \dots, z_N]^T,\ \mathbf{s}_k \in \mathbb{R}^{3N}$$

The mean shape of the training population is computed as:

$$\bar{\mathbf{s}} = \frac{1}{M}\sum_{k=1}^{M} \mathbf{s}_k\,,$$

The covariance matrix is defined as:

$$\mathbf{C} = \frac{1}{M-1}\sum_{k=1}^{M} (\mathbf{s}_k - \bar{\mathbf{s}})(\mathbf{s}_k - \bar{\mathbf{s}})^T.$$

Eigen-decomposition of $\mathbf{C}$ yields:

$$\mathbf{C} = \mathbf{U}\boldsymbol{\Lambda}\mathbf{U}^T,$$

where $\mathbf{U}$ contains the eigenvectors (i.e., the principal modes of variation) and $\boldsymbol{\Lambda}$ is the diagonal matrix of corresponding eigenvalues. Retaining the first m modes of variation defines a low-dimensional generative mode

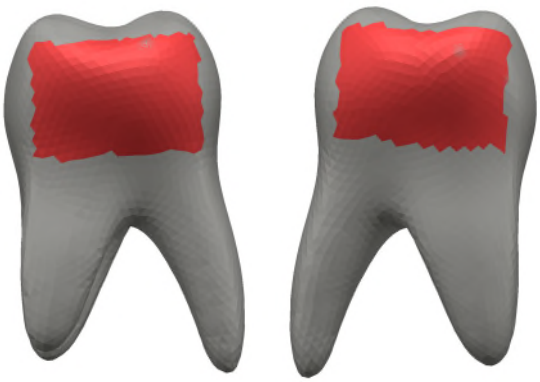
$$\mathbf{s}(\boldsymbol{\alpha}) = \bar{\mathbf{s}} + \mathbf{U}\boldsymbol{\Lambda}^{\mathbf{1/2}}\boldsymbol{\alpha} = \bar{\mathbf{s}} + \mathbf{D}\boldsymbol{\alpha}, \mathbf{D} \in \mathbb{R}^{3N\times m}, \boldsymbol{\alpha}\in\mathbb{R}^m \quad (1)$$

Each shape parameter α_k is constrained to the interval $[-3, 3]$, capturing approximately 99.7% of the population variability under the Gaussian assumption and ensuring anatomically plausible shapes. The number of retained modes satisfies:

$$m \le \mathrm{rank}(\mathbf{C}) \le \min(3N, M-1)$$

2.3 Semantic enrichment of the eSSM

The eSSM extends the classical SSM by encoding additional anatomical and functional information beyond sole geometry. In this work, the enhanced model serves two main purposes: (i) the identification of tooth regions potentially unreliable due to contact with adjacent teeth; and (ii) the automatic semantic segmentation of distinct anatomical regions. To enable anatomy-aware processing, the lateral faces of the tooth (adjacent to neighboring teeth) are identified through a binary vertex labeling of the mean shape: 0 for lateral-face points and 1 otherwise (Figure 2). This information is stored as an additional column appended to the mean shape representation $e\bar{\mathbf{s}}$. For semantic anatomical segmentation, three major regions are identified and encoded: the occlusal region, mesial region, and roots, assigned labels 1, 2, and 3, respectively (Figure 3). As for the contact-related labels, this information is stored in an additional column of the enhanced mean shape $e\bar{\mathbf{s}}$. Finally, a sixth column is used to encode the tooth class. Since a dedicated eSSM must be constructed for each tooth type, this encoding enables the automatic selection of the appropriate eSSM based on the target tooth class. As a result, $e\bar{\mathbf{s}}$ contains six columns: the original 3D coordinates and three additional label fields. Importantly, the manual annotation required to define these labels is performed only once during model construction. During fitting and target reconstruction, only the geometric coordinates are updated, while semantic labels remain fixed and are automatically transferred to the reconstructed models.



a) b)

Fig. 2 Views of lateral faces adjacent to neighboring teeth (red), encoded in the fourth column of the eSSM



Fig. 3 The semantic regions of the first molar encoded in the fifth column of the eSSM: roots (yellow), mesial region (light blue), occlusal region (dark blue)

2.4 Identification of unreliable regions on the target model

The identification of morphologically reliable and unreliable regions is a critical step of the proposed framework and is performed using an anatomy-aware and geometry-driven strategy. Let $\mathbf{s}_0$ denote the preliminary tooth reconstruction, represented as a Point Distribution Model (PDM). The framework is independent of the acquisition technology or the segmentation method used to generate $\mathbf{s}_0$, provided that a discrete representation is available. As a preprocessing step, $\mathbf{s}_0$ is brought into dense correspondence with the enhanced mean shape $e\bar{\mathbf{s}}$, ensuring a direct row-wise correspondence between the two matrices. An initial classification of unreliable regions is obtained by transferring the semantic labels stored in the fourth column of $e\bar{\mathbf{s}}$ to the target shape. Points corresponding to lateral faces (label 0) are marked as unreliable, while all remaining points are considered reliable. To further assess geometric consistency, local surface orientation is evaluated by comparing the surface normals of the preliminary reconstruction with those predicted by the statistical model. Let $\mathbf{V}_{\mathbf{s}_0} \in \mathbb{R}^{N\times 3}$ denote the vertices of the preliminary reconstruction and $\mathbf{V}_{e\bar{\mathbf{s}}} \in \mathbb{R}^{N\times 3}$ those of the shape reconstructed from the eSSM. For each vertex i, the corresponding unit normals $\mathbf{n}_{\mathbf{s}_0}^{(i)}$ and $\mathbf{n}_{e\bar{\mathbf{s}}}^{(i)}$ are computed following the method in [42]. The angular deviation between the two normals is quantified as:

$$\theta_i = \arccos\left(\mathbf{n}_{\mathbf{s}_0}^{(i)} \cdot \mathbf{n}_{e\bar{\mathbf{s}}}^{(i)}\right)$$

A vertex is classified as reliable if:

$$\theta_i < \theta_{\text{th}}$$

where θ_{th} is a predefined angular threshold. Based on preliminary tuning experiments, $\theta_{\text{th}} = 20°$ was selected and used consistently across all experiments. The resulting reliability set is defined as

$$\mathcal{R} = \{i \in \{1,\dots,N\} \mid e\bar{\mathbf{s}}(i,4) = \mathbf{1} \wedge \theta_i < \theta_{\text{th}}\} \quad (2)$$

where $e\bar{\mathbf{s}}(i,4)$ is the value in the i row and 4th column of $e\bar{\mathbf{s}}$.

2.5 Iterative eSSM Fitting and Convergence

The completion of unreliable regions is performed through an iterative eSSM fitting procedure formulated on a reduced target representation, as summarized in pseudocode reported in Algorithm 1. At each iteration, only the subset of reliable points $\mathcal{R}$ is used to constrain the fitting, while the remaining regions are inferred through statistical shape completion. Given the vectorized preliminary reconstruction $\mathbf{s}_0 \in \mathbb{R}^{3N}$, a reduced observation vector $\mathbf{s}_0^{\mathcal{R}} \in \mathbb{R}^{3|\mathcal{R}|}$ is constructed by retaining only the coordinates of reliable points. Consistently, reduced versions of the mean shape and deformation matrix, $\bar{\mathbf{s}}^{\mathcal{R}}$ and $\mathbf{D}^{\mathcal{R}}$, are obtained by selecting the corresponding rows. During the fitting process, only the first three columns of $e\bar{\mathbf{s}}$ (the spatial coordinates) are involved. Since these coincide with $\bar{\mathbf{s}}$, the mean shape is denoted simply as $\bar{\mathbf{s}}$. At each iteration t, the shape parameters $\boldsymbol{\alpha}^{(t)}$ are estimated by solving the following:

$$\boldsymbol{\alpha}^{(t)} = \underset{\boldsymbol{\alpha}}{\text{argmin}} \parallel \mathbf{s}_0^{\mathcal{R}} - (\bar{\mathbf{s}}^{\mathcal{R}} + \mathbf{D}^{\mathcal{R}}\boldsymbol{\alpha}) \parallel_2^2 + \gamma \parallel \boldsymbol{\alpha} \parallel_2^2,$$

where the regularization parameter γ enforces anatomical plausibility and numerical stability. Consistent with the MAP formulation, the regularization parameter γ was estimated from the training dataset as the variance of the residual geometric error between each training shape and its projection onto the statistical shape space. The solution is additionally constrained such that each coefficient satisfies $\mid \alpha_k \mid \leq \tau$, with $\tau = 3$, enforcing anatomical plausibility under the Gaussian assumption of the model. Once the optimal parameters are estimated, the completed tooth morphology is reconstructed as:

$$\hat{\mathbf{s}}^{(t)} = \bar{\mathbf{s}} + \mathbf{D}\boldsymbol{\alpha}^{(t)}.$$

Point-wise deviations between $\hat{\mathbf{s}}^{(t)}$ and $\mathbf{s}_0$ are then evaluated in a statistically normalized space, and the reliability set $\mathcal{R}$ is updated accordingly using Eq. (2). These deviations are explicitly used to reclassify each vertex as reliable or unreliable. The procedure is repeated until convergence, which is reached when the relative change in the shape parameters satisfies:

$$\| \boldsymbol{\alpha}^{(t)} - \boldsymbol{\alpha}^{(t-1)} \|_2 / (\| \boldsymbol{\alpha}^{(t-1)} \|_2 + 10^{-8}) < \varepsilon$$

In this work, $\varepsilon = 10^{-3}$. In practice, convergence is achieved in a small number of iterations, indicating stable identification of unreliable regions and consistent statistical completion.

Algorithm 1: Iterative eSSM-Based Statistical Shape Completion

Input:

- Preliminary reconstruction $s_0 \in \mathbb{R}^{3N}$;
- mean shape $\bar{s} \in \mathbb{R}^{3N}$;
- deformation matrix $D \in \mathbb{R}^{3N \times m}$;
- initial reliability set $R^{(0)}$;
- regularization parameter γ;
- coefficient bound $\tau = 3$;
- convergence threshold $\varepsilon = 10^{-3}$.

Output:

- Completed shape $\hat{s} \in \mathbb{R}^{3N}$.

1. Initialize $t \leftarrow 0$, $\alpha^{(0)} \leftarrow 0$
2. Repeat
   - 2.1: Construct reduced observation $s_0^{R(t)}$ by selecting coordinates in $R^{(t)}$
   - 2.2: Construct reduced mean shape $\bar{s}^{R(t)}$ and deformation matrix $D^{R(t)}$
   - 2.3: Estimate shape parameters by solving: $\alpha^{(t)} \leftarrow \text{argmin}_\alpha \| s_0^{R(t)} - (\bar{s}^{R(t)} + D^{R(t)} \alpha) \|_2^2 + \gamma \|\alpha\|_2^2$
   - 2.4: Enforce bounds: $\alpha_k^{(t)} \leftarrow \text{clip}(\alpha_k^{(t)}, -\tau, \tau), \forall k$
   - 2.5: Reconstruct full shape: $\hat{s}^{(t)} \leftarrow \bar{s} + D\,\alpha^{(t)}$
   - 2.6: Compute normalized point-wise deviations between $\hat{s}^{(t)}$ and s_0
   - 2.7: Update reliability set $R^{(t+1)}$ according to Eq. (2)
   - 2.8: $t \leftarrow t + 1$
3. Until $\|\alpha^{(t)} - \alpha^{(t-1)}\|_2 / (\|\alpha^{(t-1)}\|_2 + 10^{-8}) < \varepsilon$
4. Return $\hat{s} \leftarrow \hat{s}^{(t)}$

2.6 Target representation and partial-shape conditioning

While the eSSM is trained on complete tooth anatomies derived from CBCT data, the target geometries provided to the reconstruction pipeline may be partial, depending on the acquisition modality. In particular, intraoral scanners capture only the portion of the tooth exposed above the gingival margin, leaving the subgingival anatomy unobserved [43]. To enable effective fitting of the eSSM on this limited yet fully observed portion of the target surface, a preliminary alignment and reduction step is performed.

First, the acquired points are roughly aligned to the eSSM mean shape using a coarse manual registration. Then, a reduced target representation is generated by selecting the observed points and their local neighborhood using a k-nearest neighbors (k-NN) approach. This reduced model provides a limited but informative subset of the tooth geometry that can reliably constrain the initial fitting of the eSSM. Using these points, an initial full-shape reconstruction is obtained via a MAP estimation in the statistical shape space, producing a preliminary complete model that respects the observed crown geometry and the anatomical prior encoded in the eSSM.

The reliable subset of the extracted crown surface serves as conditioning data for the full iterative reconstruction pipeline. Consistent with the proposed approach, rather than performing local surface completion, the full tooth shape is inferred as a global deformation of the mean shape, constrained by the observed points. At each iteration, the eSSM fitting enforces strict agreement with the reliable crown points while simultaneously predicting the shape of unobserved regions according to the population-level variability encoded in the model. This ensures that reconstructed regions are consistent with both the acquired data and the anatomical prior, maintaining smoothness and structural plausibility across the entire tooth surface. Although the partial target provides fewer points than a complete geometry, the reconstruction remains well-posed due to the low-dimensional statistical shape space and the strong anatomical regularization provided by the eSSM. The principal modes of variation learned from the CBCT population restrict the solution to anatomically plausible configurations, preventing unstable extrapolations even when large portions of the tooth are unobserved. This strategy enables robust reconstruction of complete tooth models from partial surfaces while preserving fidelity to the observed crown and ensuring global anatomical coherence.

3 Results and Discussion

To demonstrate the effectiveness of the proposed anatomy-aware refinement framework, the complete pipeline was implemented in MATLAB using two custom scripts. The first script constructs the eSSM starting from a set of training shapes aligned to a common reference frame. The second script performs segmentation refinement and shape completion, taking as input a preliminary tooth reconstruction $\mathbf{s}_0$, previously aligned to the eSSM mean shape, and producing a fully reconstructed and semantically labeled tooth model. No user interaction is required during the execution of either script, except for a

one-time manual annotation step performed on the eSSM mean shape to define the additional information encoded in the fourth to sixth columns of the enhanced model (as described in Section 2.2). Both the construction of the eSSM and the associated manual annotation are performed only once. Once trained, the eSSM can be reused to refine and complete any target tooth reconstruction of the same anatomical class, independently of the acquisition modality or segmentation strategy used to generate the preliminary input. As expected, a distinct eSSM must be trained for each tooth class to ensure anatomical consistency. In the present study, the proposed pipeline was demonstrated on a single tooth class, namely the adult maxillary first upper molar. This choice is intended to illustrate the behavior and performance of the method and does not limit its general applicability to other tooth types. The selected tooth class is particularly challenging due to its complex occlusal morphology, multiple roots, and frequent interproximal contacts, making it suitable for evaluating reconstruction robustness under demanding anatomical conditions. The size of the training dataset is consistent with the statistical modelling framework adopted in this work, as population-based shape models are designed to operate with limited but anatomically consistent samples. Nevertheless, the current validation does not aim to demonstrate statistical generalizability across the entire dentition. Rather, it provides a proof-of-concept evaluation of the proposed refinement strategy. Extension to additional tooth classes and larger datasets will be addressed in future work by constructing tooth-specific eSSMs and evaluating reconstruction performance across broader anatomical variability.

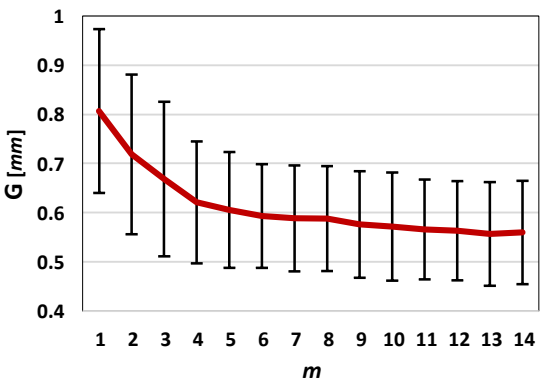
3.1 The eSSM Construction

The eSSM was trained on a limited but anatomically consistent dataset consisting of 16 complete CBCT-derived segmentations of adult maxillary first molars. The CBCT volumes were obtained from the publicly available MMDental repository [44]. Training samples were selected exclusively from scans in which complete tooth segmentation was feasible, ensuring reliable and anatomically accurate surface representations suitable for statistical modelling. Segmentations were performed using 3D Slicer through semi-automatic techniques, including thresholding. Each segmented tooth was exported as a PDM in STL format and further processed in Geomagic Design X® to correct surface defects and enforce uniform remeshing. A deviation analysis confirmed that remeshing introduced errors within ±0.1 mm. All samples were subsequently rigidly aligned to a common reference frame. Following preprocessing, all remaining steps of the eSSM construction were carried out using a custom MATLAB script. The aligned training samples were provided as input, and the resulting statistical shape model was generated automatically without further user interaction.

Given the limited size of the training dataset, all available modes of variation were retained, resulting in $m = 15$ modes. The quality of the resulting SSM was assessed using the standard evaluation metrics proposed by Davies [45]. Generalization Ability $G(m)$, Specificity $S(m)$, and Compactness $C(m)$. In this application, the metrics have been defined as follows: $G(m)$ was evaluated through a leave-one-out strategy on the training set and quantified using the Mean Absolute Deviation (MAD) computed as the average point-wise Euclidean distance between the reconstructed shape and the original shape, normalized by the number of vertices.

As a consequence, $G(m)$ represents the expected fitting error when the model is used to approximate unseen shapes. $S(m)$ was computed by generating 100,000 synthetic shapes from the model and measuring their deviation from the closest training samples. $C(m)$ quantified the cumulative variance captured by the retained modes. As shown in Figure 4, both $G(m)$ and $S(m)$ exhibit stable and consistent trends, supporting the reliability of the constructed model. Despite the limited size of the training set, the fitting accuracy quantified by $G(m)$ is approximately 0.56 mm, which is fully adequate for the intended application. To construct the enhanced version of the model, the SSM mean shape was imported into Geomagic Design X®, where relevant anatomical regions were manually segmented as described in Section 2.2.

These regions were exported as independent STL files and subsequently encoded into the eSSM through a custom MATLAB script by populating the fourth, fifth, and sixth columns of the enhanced mean shape.



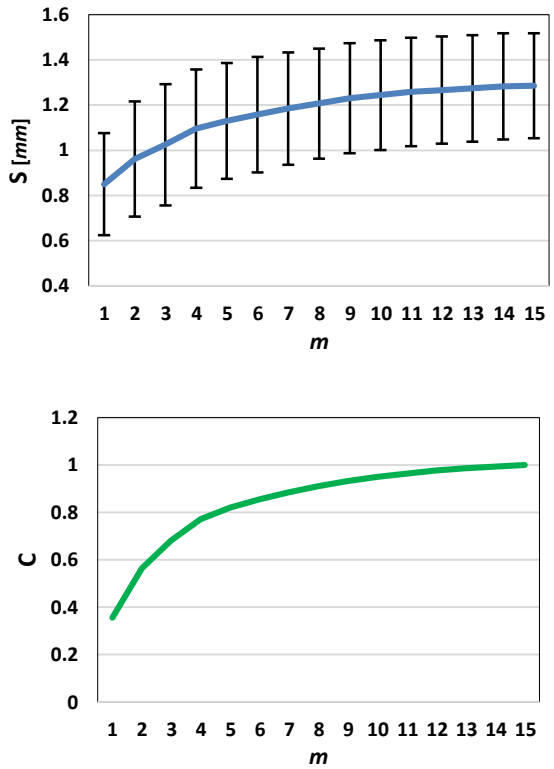


Fig. 4 The evaluation metrics G(m) and S(m) and C(m)

3.2 Application of the tooth reconstruction pipeline to the upper first molar

The proposed reconstruction pipeline was evaluated on a test set of 10 adults maxillary first molars. Five samples were obtained from CBCT scans available in the MMDental repository, while the remaining five were derived from intraoral scans provided by the Bits2Bites Dataset [46]. None of the test samples were included in the training dataset used to construct the eSSM. For the CBCT-based cases, a preliminary segmentation of the full dental arch was first generated using 3D Slicer using a semi-automatic segmentation approach. The target molar was then approximately isolated from the neighboring teeth and exported as a triangulated STL surface. As discussed in the previous sections, although a semi-automatic segmentation strategy was adopted in this experimental evaluation, the proposed pipeline is independent of the specific segmentation method. The input model may be generated by any segmentation strategy, provided that a surface- or point-based representation of the target tooth is available. For the intraoral scan cases, STL models of the full dental arch were provided directly. The user manually performed a coarse isolation of the target molar from adjacent teeth and exported it as an individual STL surface.

All ten target tooth models were coarsely aligned to the corresponding eSSM mean shape using Geomagic Design X® to ensure a consistent initial pose. The aligned models were then processed using the proposed MATLAB-based refinement pipeline. For illustrative purposes, Figure 5 presents one representative example for each acquisition modality (CBCT and intraoral scanning); analogous qualitative behavior was consistently observed across all remaining test cases, confirming the robustness of the proposed pipeline. Figures 5a and 5b show the upper full dental arch obtained from CBCT and intraoral scanning, respectively, while Figures 5c and 5d display the extracted target molars. In Figures 5c and 5d, the inaccuracy of the preliminary segmentation at the interdental contact regions can be clearly observed. Figures 5e and 5f show the final reconstructed tooth models obtained after convergence of the iterative eSSM fitting procedure, along with their semantic segmentation.

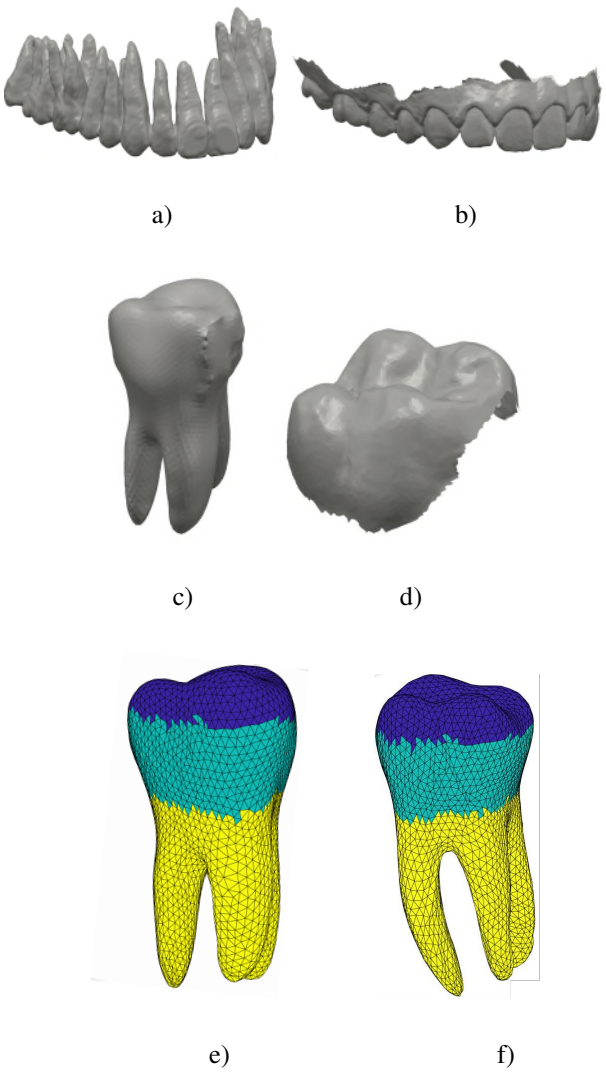
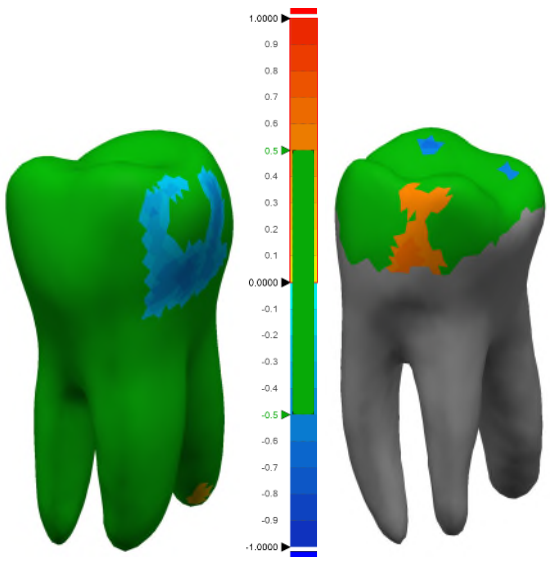


Fig. 5 Representative examples of target tooth reconstruction for both acquisition modalities. (a, b) Full upper dental arch obtained from CBCT and intraoral scanning, respectively. (c, d) Extracted target first molars, with visible inaccuracies in the preliminary segmentation at interdental contact regions. (e, f) Final reconstructed tooth models after convergence of the iterative eSSM fitting procedure, including vertex-level semantic anatomical labels

Figures 6a and 6b report the point-wise deviations between the final reconstructed models and the corresponding preliminary segmentations for the CBCT-derived and intraoral-scan-derived targets, respectively. In both cases, regions initially classified as reliable exhibit expected deviation, indicating that the observed and reliable geometry is preserved throughout the refinement process.

Conversely, larger deviations are localized in regions identified as unreliable, predominantly at interdental contact surfaces and occluded areas. These regions are reconstructed through the anatomical prior encoded in the eSSM, resulting in smooth, geometrically coherent, and anatomically plausible reconstructions. Overall, the reconstructed tooth models are complete and free of local artifacts typically associated with ambiguous or poorly constrained regions, making them directly suitable for downstream applications such as prosthetic planning, quantitative morphometric analysis, and the design and manufacturing of surgical or restorative devices. From a digital manufacturing perspective, the proposed refinement strategy is intended to generate anatomically coherent tooth geometries rather than optimize segmentation accuracy alone. This positioning reflects the role of the method as a geometry refinement step within CAD/CAM-oriented workflows, where surface continuity, morphological plausibility, and robustness to incomplete data are critical requirements [47]. Due to the limited extent of the observed crown surface, reconstruction from intraoral scans entails higher inherent uncertainty [48]; nonetheless, the pipeline preserves reliable geometry while producing a complete, anatomically coherent tooth model. The extent and spatial distribution of missing regions in intraoral scans directly influence reconstruction uncertainty. In particular, subgingival areas and interproximal contact regions are typically unobserved [48], requiring the reconstruction to rely primarily on the statistical prior encoded in the eSSM. In the proposed framework, this uncertainty is implicitly handled through the reliability classification step, which preserves observed geometry while constraining completion to anatomically plausible variations. However, a systematic sensitivity analysis evaluating reconstruction stability across different missing-data patterns was not conducted in this study. Such analysis could be conducted in future work by progressively masking observed crown regions, simulating varying levels of occlusion, or artificially removing surface patches to quantify the impact on reconstruction variability. This would enable explicit estimation of uncertainty bounds associated with intraoral-scan–derived reconstructions.

A direct quantitative validation against a ground-truth geometry is not reported, as the true original tooth morphology is inherently unobservable in clinical scenarios, particularly in regions affected by contact or occlusion [49, 50]. Alternative validation strategies could be considered in future work to provide a complementary quantitative assessment. These may include the use of physical dental phantoms with known geometry, ex vivo teeth digitised using high-precision laboratory scanners, or multimodal acquisitions combining CBCT with industrial-grade optical scanning. Such approaches would enable controlled evaluation of reconstruction accuracy in both observed and reconstructed regions. In addition, application-driven benchmarks based on downstream CAD/CAM tasks, such as surgical guide fitting accuracy, occlusal contact consistency, or restoration design robustness, could provide task-oriented validation of the proposed refinement strategy in manufacturing workflows. Moreover, the primary objective of the proposed method is not to recover an exact but unknown ground truth, but rather to generate anatomically consistent reconstructions that strictly preserve reliable observed regions while plausibly completing uncertain or missing areas. In this context, the qualitative preservation of trustworthy geometry, combined with statistically grounded shape completion, provides a meaningful and application-oriented assessment of the effectiveness of the proposed pipeline.



a) b)

Fig. 6 The point-wise deviations between the final reconstructed models and the corresponding preliminary segmentations for the targets derived from (a) CBCT (maximum deviations: +0.67, -0.62) and (b) intraoral scan (maximum deviations +0.53, -0.83)

4 Conclusions

In this work, a fully automated pipeline for tooth reconstruction and segmentation refinement based on an eSSM has been presented. The approach functions as a refinement stage within broader digital workflows, taking

as input a preliminary tooth segmentation (regardless of acquisition modality or segmentation strategy) and producing complete, anatomically coherent models suitable for downstream design and manufacturing applications. The eSSM extends classical SSMs by embedding semantic and functional information directly into the mean shape, including anatomy-aware labels and region-specific encoding. Combined with a geometry-driven reliability assessment that compares local surface orientation against the anatomical variability captured by the eSSM, this framework explicitly identifies reliable and uncertain regions. Reliable areas are strictly preserved, while ambiguous or missing regions are reconstructed using population-level anatomical priors, effectively mitigating limitations associated with incomplete data, segmentation artifacts, and acquisition uncertainties. The method was evaluated on ten adult maxillary first molars (five CBCT-derived and five intraoral scan-derived cases).

The maxillary first molar was selected due to its anatomical complexity, making it a challenging and representative test case. The results thus guides, demonstrate consistent preservation of reliable surfaces and anatomically plausible reconstruction of uncertain regions across both acquisition types, confirming the robustness of the pipeline under heterogeneous input conditions. A direct quantitative validation against ground-truth geometry was not possible, as the true morphology is inherently unobservable in clinical scenarios. However, the approach prioritizes the generation of anatomically plausible, structurally coherent, and functionally adequate reconstructions, making it suitable for design, planning, and manufacturing applications [51]. In a manufacturing-oriented workflow, the proposed eSSM-based refinement can be applied to generate reliable tooth geometries for the automated design and fabrication of tooth-supported surgical guides, thereby reducing manual intervention, time-consuming process and operator variability [52] while improving geometric consistency and fit accuracy. Future work will focus on extending the framework to additional tooth classes, increasing the anatomical variability of training datasets, automating initialization and alignment procedures, and integrating partial-surface data more systematically. The adoption of this pipeline in end-to-end digital dental workflows represents a promising avenue for robust, automated manufacturing-oriented reconstruction.

Statements & Declarations

The authors declare that no funds, grants, or other support were received during the preparation of this manuscript.

Funding

The authors declare that no funds, grants, or other support were received during the preparation of this manuscript.

Competing Interests

The authors declare that they have no financial conflicts of interest related to this work.

Author Contributions

All authors contributed to the conception and design of the study. Material preparation, data collection, and formal analysis were performed by Marzola A., Baiamonte G., and Monaco F.C.R. The first draft of the manuscript was written by Baiamonte G. and Marzola A., and all authors provided comments and revisions on previous versions of the manuscript. The final revision and supervision were carried out by Di Angelo L. and Calì M. All authors read and approved the final version of the manuscript.

References

1. Baiamonte, G., Pascoletti, G., Monaco, F., Calì, M., & Zanetti, E. M. (2025, June). Emerging Technologies and Performing Materials in Manufacturing Dental Prostheses: The Role of Chewing Simulators. In International Conference on Flexible Automation and Intelligent Manufacturing (pp. 375-383). Cham: Springer Nature Switzerland.
2. Gómez, M. M., Guerrero-Torres, M., Villarreal-Archila, S. M., & Rodríguez, J. N. (2025). Assessing the Impact of Additive Manufacturing on Dental Clinical Workflows: A Process-Oriented Approach. *Journal of Composites Science*, *9*(11), 579.
3. Hassan, B., Souza, P. H. C., Jacobs, R., Berti, S. de A., & Stelt, P. F. van der. (2009). Influence of scanning and reconstruction parameters on quality of three-dimensional surface models of the dental arches from cone beam computed tomography. *Clinical Oral Investigations*, *14*(3), 303.
4. Azpiazu-Flores, F. X., Johnston, W. M., Morton, D., Lin, W., & Yılmaz, B. (2024). Trueness of the apical and middle root portion segments of 3D-printed removable die and alveolar cast designs manufactured using stereolithographic 3D printing. Journal of Prosthodontics.
5. Gil, I., Rodríguez, V., Arribas, C. T., Mosaddad, S. A., Peláez, J., & Suárez, M. J. (2025). Effect of 3D printing technology, build orientation, and shell thickness on the accuracy of full-arch dental models for fixed dental prostheses: an in vitro study. *Scientific Reports*, *15*(1), 40938.
6. Alghauli, M. A., Aljohani, W., Almutairi, S., Aljohani, R., & Alqutaibi, A. Y. (2025). Advancements in digital data acquisition and CAD technology in Dentistry: Innovation, clinical Impact, and promising integration of artificial intelligence. *Clinical eHealth*, *8*, 32.
7. Jani, G., Lavin, W. S., Ludhwani, S., & Johnson, A. (2021). An Overview of Three Dimensional (3D) Technologies in Forensic Odontology. *Journal of Forensic Dental Sciences*, 18.
8. Scarfe WC, Farman AG (2008) What is Cone-Beam CT and How Does it Work? Dent Clin North Am 52:707–730. https://doi.org/10.1016/j.cden.2008.05.005
9. Pauwels R, Araki K, Siewerdsen JH, Thongvigitmanee SS (2015) Technical aspects of dental CBCT: state of the art. Dentomaxillofacial Radiology 44:20140224. https://doi.org/10.1259/dmfr.20140224
10. Hao, J., Kang, Y., Wei, S., Wang, J., & Wang, H. (2024). 3D intraoral scanning techniques support the effects of crown

morphology on dental caries. *BMC Oral Health*, *24*(1).
11. Putrino, A., Bruti, V., Marinelli, E., Ciallella, C., Barbato, E., & Galluccio, G. (2020). Intraoral Scanners in Personal Identification of Corpses: Usefulness and Reliability of 3D Technologies in Modern Forensic Dentistry. *The Open Dentistry Journal*, *14*(1), 255.
12. Marzola, A., Robilotta, C., Volpe, Y., Governi, L., & Furferi, R. (2020). Statistical Shape Model: comparison between ICP and CPD algorithms on medical applications. *International Journal on Interactive Design and Manufacturing (IJIDeM)*, *15*(1), 85.
13. Im, J., Kim, J.-Y., Yu, H., Lee, K., Choi, S., Kim, J.-H., Ahn, H.-K., & Cha, J. (2022). Accuracy and efficiency of automatic tooth segmentation in digital dental models using deep learning. *Scientific Reports*, *12*(1)
14. Zhou, Y., Xu, Y., Khalil, B., Nalley, A., & Tarce, M. (2025). An open deep learning-based framework and model for tooth instance segmentation in dental CBCT. *Clinical Oral Investigations*, *29*(10).
15. Brahmi, W., Jdey, I., & Drira, F. (2024). Exploring the role of Convolutional Neural Networks (CNN) in dental radiography segmentation: A comprehensive Systematic Literature Review. *Engineering Applications of Artificial Intelligence*, *133*, 108510.
16. Broll A, Goldhacker M, Hahnel S, Rosentritt M (2024) Generative deep learning approaches for the design of dental restorations: A narrative review. J Dent 145:104988. https://doi.org/10.1016/j.jdent.2024.104988
17. Zhang H, Yuan T, Li T, et al (2025) A review of tooth AI segmentation on medical data. Discover Imaging 2:17. https://doi.org/10.1007/s44352-025-00021-2
18. Polizzi A, Quinzi V, Ronsivalle V, et al (2023) Tooth automatic segmentation from CBCT images: a systematic review. Clin Oral Investig 27:3363–3378. https://doi.org/10.1007/s00784-023-05048-5
19. Kot WY, Au Yeung SY, Leung YY, et al (2025) Evolution of deep learning tooth segmentation from CT/CBCT images: a systematic review and meta-analysis. BMC Oral Health 25:800. https://doi.org/10.1186/s12903-025-05984-6
20. Takeya, A., Watanabe, K., & Haga, A. (2024). Fine structural human phantom in dentistry and instance tooth segmentation. *Scientific Reports*, *14*(1).
21. Ma, T., Wei, X., Zhai, J., Zhang, Z., Li, Y., & Li, Y. (2025). Feature-guided multilayer encoding–decoding network for segmentation for 3D intraoral scan data. *Scientific Reports*, *15*(1).
22. Zhu, Y., Kéchichian, R., Richert, R., Ikehata, S., & Valette, S. (2026). High-Fidelity 3D Tooth Reconstruction by Fusing Intraoral Scans and CBCT Data via a Deep Implicit Representation. *arXiv (Cornell University)*.
23. Ya-Li Song, Jia Li, Tian Huang, Ping Gao (2005) The Feature-Based Modeling of Standard Tooth in a Dental Prosthetic Database. In: 2005 IEEE Engineering in Medicine and Biology 27th Annual Conference. IEEE, pp 6930–6933
24. Song Y-L, Li J, Yin L, et al (2007) The feature-based posterior crown design in a dental CAD/CAM system. The International Journal of Advanced Manufacturing Technology 31:1058–1065. https://doi.org/10.1007/s00170-005-0289-1
25. Fan L, Xiong T, Li J, Bu N (2024) Research on Denture Modeling Method Based on NURBS Curve Fitting Algorithm. In: 2024 3rd International Conference on Artificial Intelligence and Computer Information Technology (AICIT). IEEE, pp 1–4
26. Martorelli, M., & Ausiello, P. (2013). A novel approach for a complete 3D tooth reconstruction using only 3D crown data. International Journal on Interactive Design and Manufacturing (IJIDeM), 7(2), 125-133.
27. Schnitzhofer K, Rauch A, Schmidt M, Rosentritt M (2023) Impact of the occlusal contact pattern and occlusal adjustment on the wear and stability of crowns. J Dent 128:104364. https://doi.org/10.1016/j.jdent.2022.104364
28. Qian, J., Lu, S., Gao, Y., Tao, Y., Lin, J., & Lin, H. (2021). An automatic tooth reconstruction method based on multimodal data: J. Qian et al. Journal of Visualization, 24(1), 205-221.
29. Liu, J., Hao, J., Lin, H., Pan, W., Yang, J., Feng, Y., Wang, G., Li, J., Jin, Z., Zhao, Z., & Liu, Z. (2023). Deep learning-enabled 3D multimodal fusion of cone-beam CT and intraoral mesh scans for clinically applicable tooth-bone reconstruction. *Patterns*, 4(9), 100825.
30. Knoops, P. G. M., Borghi, A., Breakey, R. W. F., Ongkosuwito, E. M., & Swennen, G. R. J. (2021). Three-dimensional fusion of intraoral scans and cone-beam computed tomography scans for virtual surgical planning: accuracy of commercially available software. *Clinical Oral Investigations*, 25, 77–85.
31. Marzola A, Di Angelo L, Di Stefano P, Volpe Y (2024) An enhanced statistical shape model for automatic feature segmentation of human vertebrae. Biomed Signal Process Control 91, https://doi.org/10.1016/j.bspc.2024.105972
32. Buchaillard SI, Ong SH, Payan Y, Foong K (2007) 3D statistical models for tooth surface reconstruction. Comput Biol Med 37:1461–1471 https://doi.org/10.1016/j.compbiomed.2007.01.003
33. Soltaninejad MR, Zoroofi RA, Shirani G (2012) Automatic crown surface reconstruction using tooth statistical model for dental prosthesis planning. In: 2012 19th Iranian Conference of Biomedical Engineering (ICBME). IEEE, pp 218–222
34. Woods C, Fernee C, Browne M, et al (2017) The potential of statistical shape modelling for geometric morphometric analysis of human teeth in archaeological research. PLoS One 12:e0186754. https://doi.org/10.1371/journal.pone.0186754
35. Kim H-H, Choi S, Chang Y-I, et al (2022) Developing a three-dimensional statistical shape model of normal dentition using an automated algorithm and normal samples. Clin Oral Investig 27:759–772. https://doi.org/10.1007/s00784-022-04824-z
36. Jin X, Wang S, Hu J, et al (2023) Automated tooth crown design with optimized shape and biomechanics properties. Front Bioeng Biotechnol 11:1216651. https://doi.org/10.3389/fbioe.2023.1216651
37. Rahbani D, Fliss B, Ebert LC, Bjelopavlovic M (2023) Detecting missing teeth on PMCT using statistical shape modeling. Forensic Sci Med Pathol 20:23–31. https://doi.org/10.1007/s12024-023-00590-w
38. Chen Y, Gao S, Tu P, Chen X (2024) Automatic 3D Teeth Reconstruction From Five Intra-Oral Photos Using Parametric Teeth Model. IEEE Trans Vis Comput Graph 30:4780–4791. https://doi.org/10.1109/TVCG.2023.3277914
39. Marzola A., Buonamici F., Guariento L., Governi L.: Enhanced Statistical Shape Model: A Statistical-Based Tool to design Custom Orthopaedic Devices (2022) Lecture Notes in Mechanical Engineering, pp. 27 - 38; DOI: 10.1007/978-3-030-91234-5_3
40. BALKAN, E. P., İNCEBEYAZ, B., DENİZ, H. A., & Eren, H. (2023). Evaluation of the Frequency of Artifacts in CBCT Depending on the Different Size of Field of View. *European Journal of Research in Dentistry*, 8.
41. Marzola A, McGreevy KS, Mussa F, et al (2023) HyM3D: A hybrid method for the automatic 3D reconstruction of a defective cranial vault. Comput Methods Programs Biomed 234:107516. https://doi.org/10.1016/j.cmpb.2023.107516
42. Pauly M, Gross M, Kobbelt LP Efficient simplification of point-sampled surfaces. In: IEEE Visualization, 2002. VIS 2002. IEEE, pp 163–170
43. Mangano, F., Gandolfi, A., Luongo, G., & Logozzo, S. (2017). Intraoral scanners in dentistry: a review of the current literature [Review of *Intraoral scanners in dentistry: a review of the current literature*]. *BMC Oral Health*, *17*(1). BioMed Central.
44. Wang C, Zhang Y, Wu C, et al (2025) MMDental - A multimodal dataset of tooth CBCT images with expert medical

records. Sci Data 12:1172. https://doi.org/10.1038/s41597-025-05398-7
45. Davies R (2002) Learning shape: optimal models for analysing natural variability
46. Borghi L, Lumetti L, Cremonini F, et al Bits2Bites: Intra-oral Scans Occlusal Classification
47. Calatroni, L., Húska, M., Morigi, S., & Recupero, G. A. (2022). A Unified Surface Geometric Framework for Feature-Aware Denoising, Hole Filling and Context-Aware Completion. *Journal of Mathematical Imaging and Vision*, *65*(1), 82.
48. Nedelcu, R., Olsson, P., Nyström, I., & Thor, A. (2018). Finish line distinctness and accuracy in 7 intraoral scanners versus conventional impression: an in vitro descriptive comparison. *BMC Oral Health*, *18*(1).
49. Gaboutchian, A. V., Knyaz, V. A., Vasilyev, S. V., Korost, D. V., & Kudaev, A. A. (2021). Orientation vs. orientation: Image processing for studies of dental morphology. *The International Archives of the Photogrammetry, Remote Sensing and Spatial Information Sciences*, *43*, 723-728.
50. McFarlane, G., Floyd, B., Smith, C. B., & Mahoney, P. (2021). Technical note: Estimating original crown height in worn mandibular canines using aspects of dentin morphology. *American Journal of Physical Anthropology*, *176*(4), 692.
51. Quatrano, A., Fontana, C., Rubino, F., Cappetti, N., & Carlone, P. (2022). Analysis of the influence of inner morphology on blood flow in 3D-printed bone scaffolds. *Procedia CIRP*, *110*, 225-230.
52. Cappetti, N., Di Angelo, L., Fontana, C., & Marzola, A. (2025). A computer-based method for the automatic identification of the dimensional features of human cervical vertebrae. *Computer Methods and Programs in Biomedicine Update*, *7*, 100175.